



## Original Research Paper

## Flow phenomenon of micron-sized particles during cold spray additive manufacturing: High-speed optic observation and characterization



Libin Lalu Koithara, Rija Nirina Raoelison\*, Sophie Costil

Université de Bourgogne Franche-Comté - UTBM, Laboratoire Interdisciplinaire Carnot de Bourgogne, UMR 6303 CNRS, 90100 Belfort, France

## ARTICLE INFO

## Article history:

Received 17 July 2019

Received in revised form 28 November 2019

Accepted 23 December 2019

Available online 8 January 2020

## Keywords:

Cold spraying

Particle flow

High-speed visualization

Instability

Dispersion

## ABSTRACT

A high-speed laser shadowgraph observation of the particles flow during cold spraying enables a good phenomenological characterization. The particles in-flight behaviour develops a kinematics with two regimes regardless the powder nature. When leaving the nozzle, the particles form a regime of uniform jet over a certain distance along the flow direction, and then a regime of sparse jet while particles deviate in the radial direction. This dispersion increases away from the nozzle exit and exhibits thereby an event of oblique collision during an additive route process. Under such conditions, kinematic deficiency prevails since oblique collision has shown to alter the deposition efficiency, in the literature. Albeit these particles flow regimes represent a generic behaviour, there are differences in the powder's response depending of their features that can be combined using the parameter  $\rho_p D_p$ . The variance  $\rho_p D_p$  in cold spraying is scaled through a few cases of powders (copper, aluminium, magnesium, cermet, and PEEK). The powders dispersion becomes more and more important as  $\rho_p D_p$  decreases from high value (large Cu powders) down to low value (case of Mg powders). However, this tendency cannot be extrapolated to lightweight powders represented by the fine PEEK powders (low  $\rho_p D_p$ ) which are more stable over a larger distance due to a higher sensitivity to the axial component of the gas velocity. They get unstable later in the jet since they become sensitive to the radial component of the gas velocity due to a progressive decrease of the axial gas velocity. The fine WC-Co powders adopt similar behaviour since they are lightweight as the PEEK powders due to their porous structure.

© 2019 The Society of Powder Technology Japan. Published by Elsevier B.V. and The Society of Powder Technology Japan. All rights reserved.

## 1. Introduction

The cold spray additive manufacturing has been widely investigated as new coating technology [1–4]. Cold spraying (CS) falls under the category of thermal spray process, but it differs from others in terms of the state of bonding. It involves a solid-state high-strain rate bonding by means of supersonic gas flow. Micro-sized powders are accelerated by the supersonic gas cold expansion through a De Laval Nozzle, and then collide onto a substrate to generate the additive component. This low thermal deposition can prevent phase changes, thermal stresses or pores formation. Such advantages make the CS technique suitable for thermally sensitive coatings fabrication, cost-effective restoration of airframe structures and 3D additive prototyping of complex shape [2,4]. The cold spraying method is a scalable process that covers a broad range of materials including advanced or precursor materials such bulk metallic glass, carbon nanotubes, graphene and more. With

such flexibility, the cold spray additive manufacturing enables several surface functionalization for various applications with various opportunities of materials hybridizing such as oxide/polymer [5], ceramic/metal [6], metal/polymer [7–11] or polymer/metal [12,13]. Exhaustive examples reported in [1–4] show the huge application of the cold spray technology in the field of transport, energy management, sustainable, mechanical engineering and so forth. The use of pressure less than 10 bar brings new opportunities, viz thermally sensitive surface working, in-situ restoration of antique metallic sculptures, on-site restoration of functional dimension, or other applications for economic arguments [4]. Together, these capabilities have led the CS process to grow worldwide to become a new competitive additive manufacturing [2,4].

Despite these achievements, low pressure cold spraying (LPCS) cannot fulfil a need of high material raw rentability. The deposition efficiency (DE), that is the number of deposited powders, remains low, for instance 10% even lower when using low-pressure gas of 6 bar with compressed air as propellant [14], or 7% only for the LPCS manufacturing of fine aluminium powders with a typical size of 17  $\mu\text{m}$  [15]. Despite many explorations including different

\* Corresponding author.

E-mail address: [rijia-nirina.raoelison@utbm.fr](mailto:rijia-nirina.raoelison@utbm.fr) (R.N. Raoelison).

parameters combinations such as gas conditions, various nozzle dimensions and particle sizes, the DE remains low not exceeding 40% due to kinematic deficiency [14–17]. The dependence of the DE on a critical particle velocity has been established in the literature and correlated to detrimental factors such as the angular orientation of the nozzle with respect to the normal direction of the

substrate surface [18–20]. Maximizing the impact velocity implies to have a normal collision. A normal velocity component allows better material deposition and better DE. The more tilted the nozzle orientation, the less the DE, the depositing strength, the adhesion strength or the coating quality [21–26]. Thereby, a change in impact angle alters the kinematics of particles. These limitations

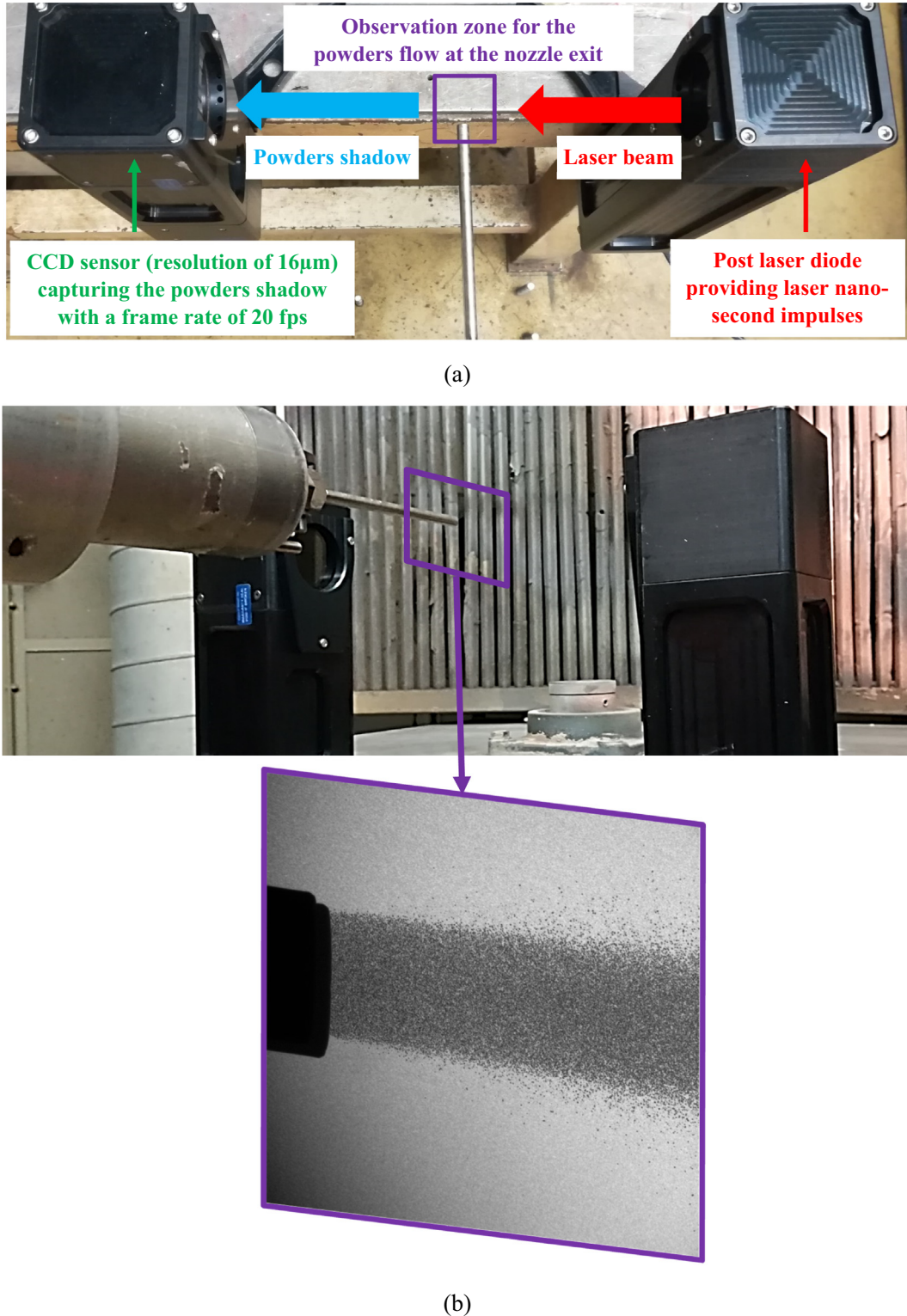


**Fig. 1.** SprayCam system and mounting for observing the particles motion: top view (a) and front view with a typical shadowgraph of the powders jet captured by the CCD sensor (b).

imply to better characterize the particle in-flight behaviour for perspectives of suitable optimized process conditions. In the literature of cold spraying, the knowledges on this aspect rather focus on the particles velocity that can be measured using DPV2000, Laser-2-Focus or laser Particle Image Velocimetry are viable for that purpose [27]. The phenomenological behaviour of the particles flows remains however a subject of deep analysis. In this paper, a high-speed laser shadowgraph is used to observe and to characterize the kinematic behaviour of particles during LPCS, and then to bring a further understanding on how the particle in-flight behaviour can be optimized.

## 2. Materials and method

### 2.1. High-speed shadowgraph observation

High-Speed shadowgraph photography enables for visualizing the behaviour of particles within the free jet. We use the system SprayCam (Control Vision Inc.) that is a laser-based particle visualization set-up. This system comprises a high-speed sensor head that captures the shadow of the particles generated by a laser diode illumination. High illumination is produced by an intense but extremely short (40 ns) laser impulse. The zone of free jet

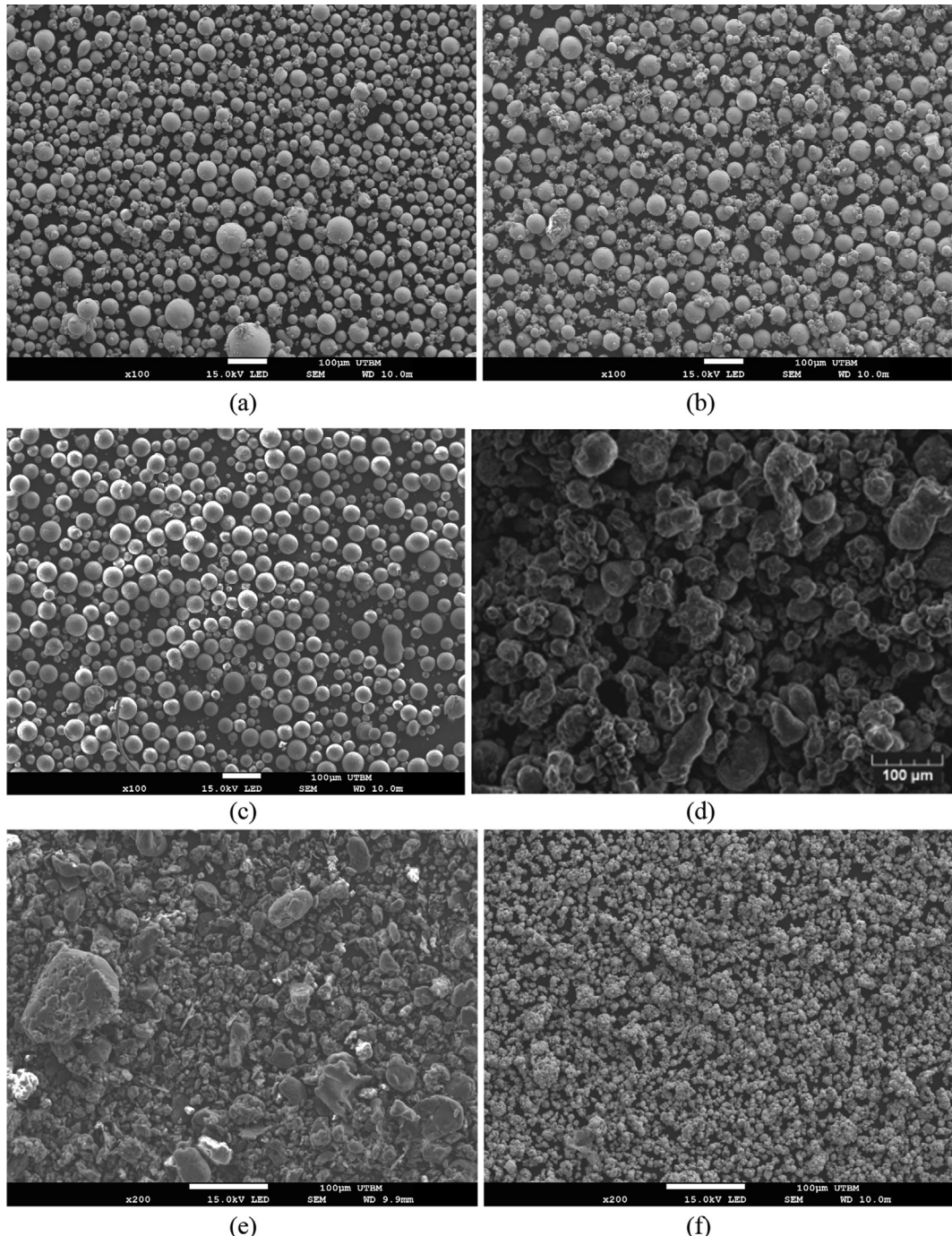


**Fig. 2.** SEM morphology of the powders: large copper powders denoted Cu\_2 (a), finer copper powders denoted Cu\_1 (b), magnesium powders (c), aluminium powders (d), PEEK powders (e), and cermet powders (f).

ahead the nozzle is then placed between the laser diode and the sensor as shown in Fig. 1 so that the sprayed micron-sized particles create a shadow by high illumination backlighting principle. This intense light source is synchronized with the high-speed CCD sensor head to capture the shadow of the micron-sized particles. The CCD resolution is 16  $\mu\text{m}/\text{pixel}$  and the capturing frame rate is 20fps. Since the observation window is limited to 15 mm length, the zone of free jet ahead the nozzle is divided into successive observation zones with an increment of 15 mm, that is 0–15 mm (zone 1), 15–30 mm (zone 2) and so forth towards zone 6 (75–90 mm). This series of observations allow for visualizing the particle flight over a large distance at the nozzle exit (0–90 mm ahead the nozzle).

## 2.2. Powders specification and LPCS condition

Typical CS powder natures are considered, from lightweight to heavy materials, and from fine to coarse powders. This representativity can be classified as follows: 30–60  $\mu\text{m}$  sized copper powders as high-density CS materials, larger copper powders (36–160  $\mu\text{m}$ ) as heavy CS powders, and PEEK powders to include the case of lightweight powders. Fine PEEK powders are used with a size range compatible with the resolution of the shadowgraph CCD system (16  $\mu\text{m}/\text{pixel}$ ). The lightweight PEEK is compared to a heavy powder (WC-Co) for the same granulometry. Since fine powders are recommended for improving the DE of LPCS, further intermediate cases of lightweight powders are included, viz. fine Al powders and fine Mg powder whose sizes are also slightly higher than the CCD resolution. Together, this powder variance provides a depiction of kinematic particle behaviour during LPCS.

The copper powders are in-house products manufactured by atomization. The other powders are marketed goods supplied by ECKA (aluminium powders), Victrex France (PEEK powders), Sulzer Metco (cermet powders) and China Lab (magnesium powders). The powders morphology is shown in Fig. 2. The granulometry detail is given in Fig. 3 and Table 1. The kinematic behaviour of these powders during cold spraying is investigated using a DYMET 423 LPCS system composed of a control unit, a vibrational powder feeder, a convergent-divergent nozzle mounted on a compact spraying gun. The steel nozzle has an inlet diameter of 8 mm, a throat diameter of 2.55 mm, an outlet diameter of 5 mm, a convergent part length of 6 mm and a divergent part length of 131 mm. The spray gun is supplied with a 6 bar non-heated nitrogen gas and the powders are radially fed into the nozzle with a powder feed rate of 5 g/min.

## 3. Results and discussions

### 3.1. Phenomenological flow the particles within the free jet

Despite they are different in size and nature, the particles adopt a similar phenomenological behaviour we can describe by the observation of the large copper case whose particle size produces clearer pictures. The location of the particles within the free jet reveals their kinematics outside the nozzle. A snapshot view on each observation zone from zone 1 to zone 6 provides a visualization of the particles that is clear in terms of instantaneous quantity and spatial distribution within the jet (Fig. 4). Each captured frame exhibits a weak presence of particles so that most of them are individually identified. They are dispersed within the jet but remain inside a flow zone which corresponds to the exit diameter of the

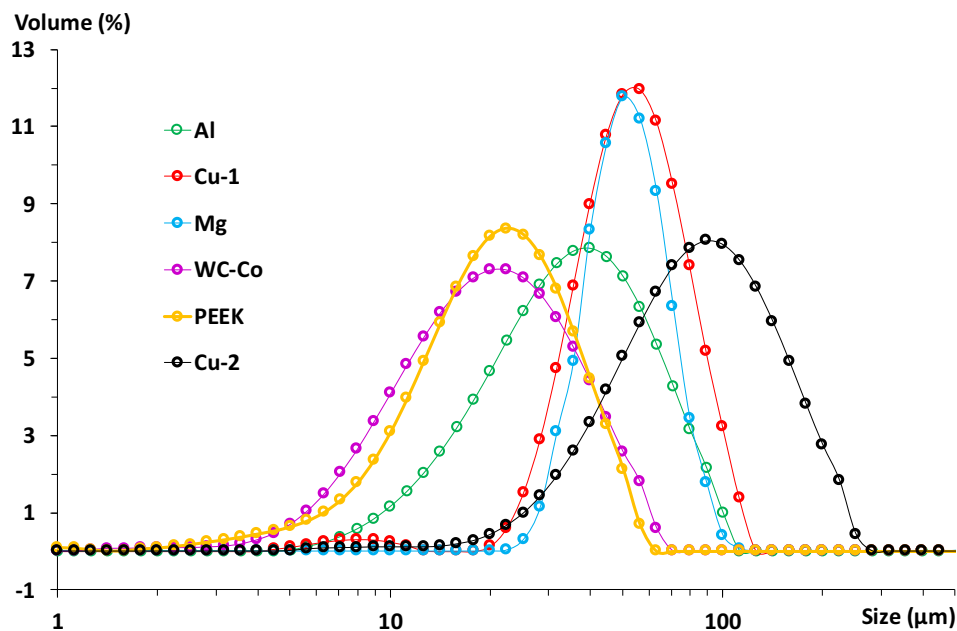
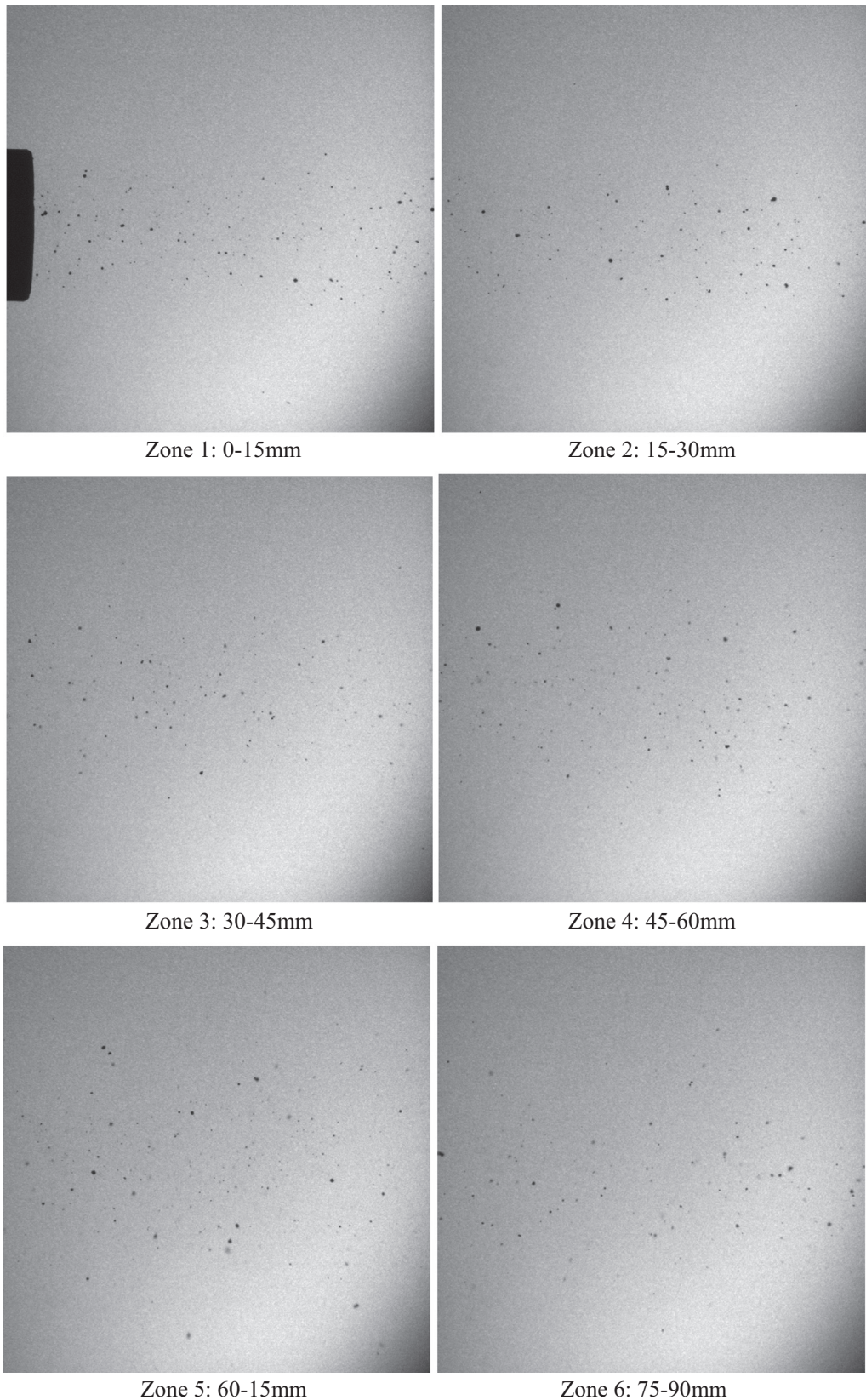


Fig. 3. Powders size distribution obtained by a Malvern Mastersizer 2000 particle size analyser.

Table 1

Particle size range measured by the Malvern Mastersizer 2000 laser granulometry system.

Powders	Cu-1	Cu-2	Al	Mg	PEEK	WC-Co
D10 ( $\mu\text{m}$ )	30.53	36.23	17.13	16.38	8.02	8.07
D50( $\mu\text{m}$ )	50.13	79.70	41.29	55.24	19.25	18.55
D90( $\mu\text{m}$ )	79.28	154.19	80.66	80.65	36.04	38.22
Size range ( $\mu\text{m}$ )	30–80	36–160	17–81	16–81	8–37	8–38



**Fig. 4.** Instantaneous particle spatial distribution within the jet: snapshot view on each observation zone from zone 1 to zone 6.

nozzle. Such confinement occurs in the immediate vicinity of the nozzle exit (zone 1 and zone 2), and then progressively disappears. From zone 3, the particles are progressively scattered showing thereby a larger dispersion zone. Thus, the particle jet becomes

radially wider along the flow direction that characterizes the typical phenomenological kinematic behaviour of CS particles during the supersonic external expansion of the gas outside the nozzle.

Stacked images reveal that over a short distance ahead of the nozzle, the particles form a jet with a uniform diameter which corresponds to the nozzle exit diameter. The sequential stacks of a few images show this uniform diameter is stable at the immediate vicinity of the nozzle exit. The particles remain inside this steady state uniform jet that characterizes a regime of stable particles

flow. Note that there is no steady state regime of each particle since the captured locations of the particles vary from one snapshot to another (Fig. 5). The individual location of the particles is not repetitive although their global motion generates the uniform and stable jet. Due to the exit supersonic velocity of the gas, the strong axial drag force confines the particles inside the exit gas

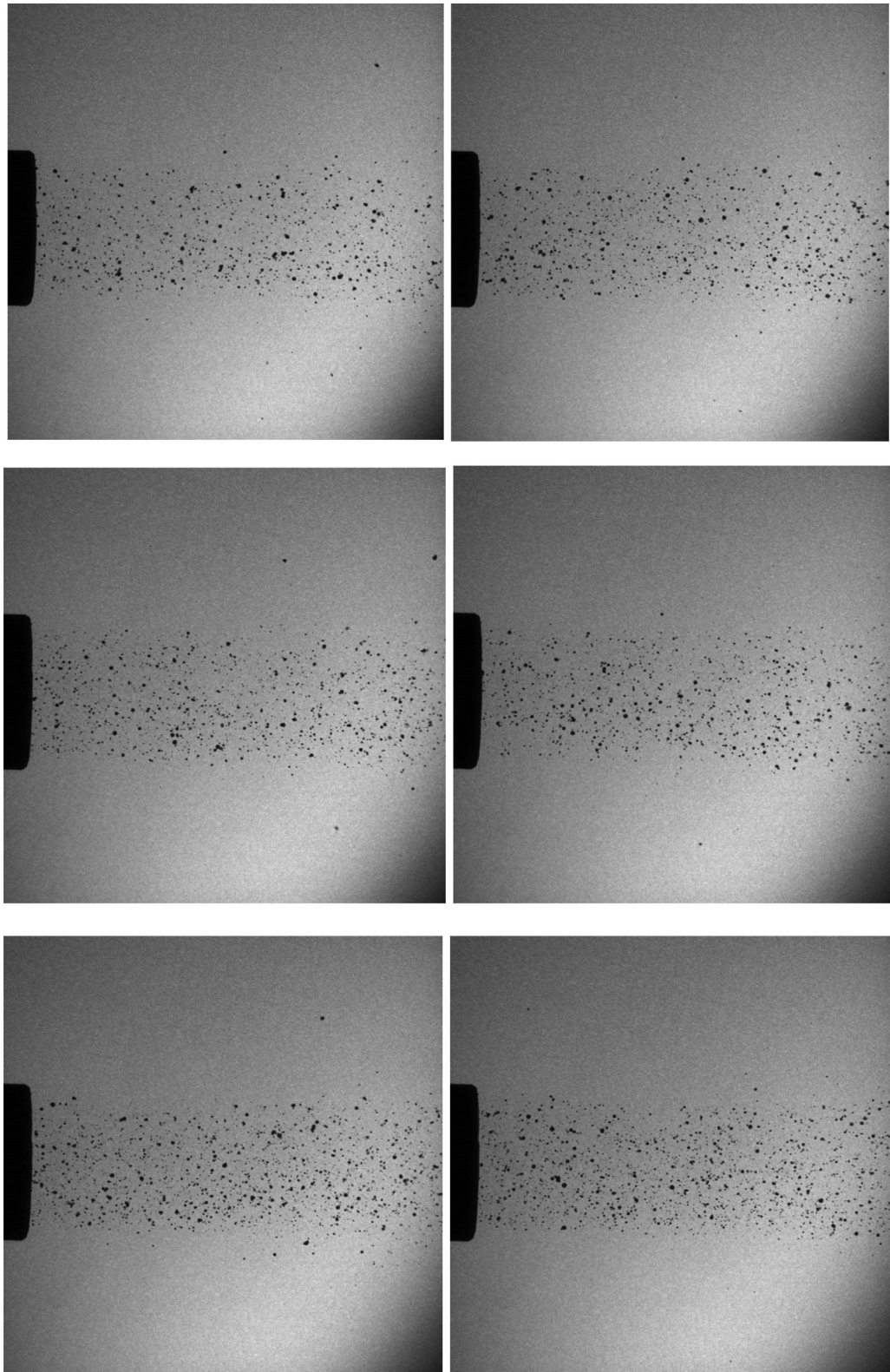


**Fig. 5.** Sequential stacking of 15 images that shows the development of typical straight jet at the nozzle exit within zone 1.

stream. However, the axial drag force is no longer predominant along the flow direction since the dispersion of particles appears while leaving the zone 1. The presence of some particles outside the central jet indicates a radial drag force component that deviates these particles. These deviations are persistent but irregular due to the random allocation of the particles within the gas stream.

The visualization through sequential snapshot shows typical randomly and non-repetitive dispersion that is developing or is fully developed such as within zone 3 (Fig. 6) and zone 5 (Fig. 7) respectively. The recurrence of this dispersion phenomenon can also arise from the development of turbulent and unstable behaviour of the gas flow outside the nozzle [28]. Because of their

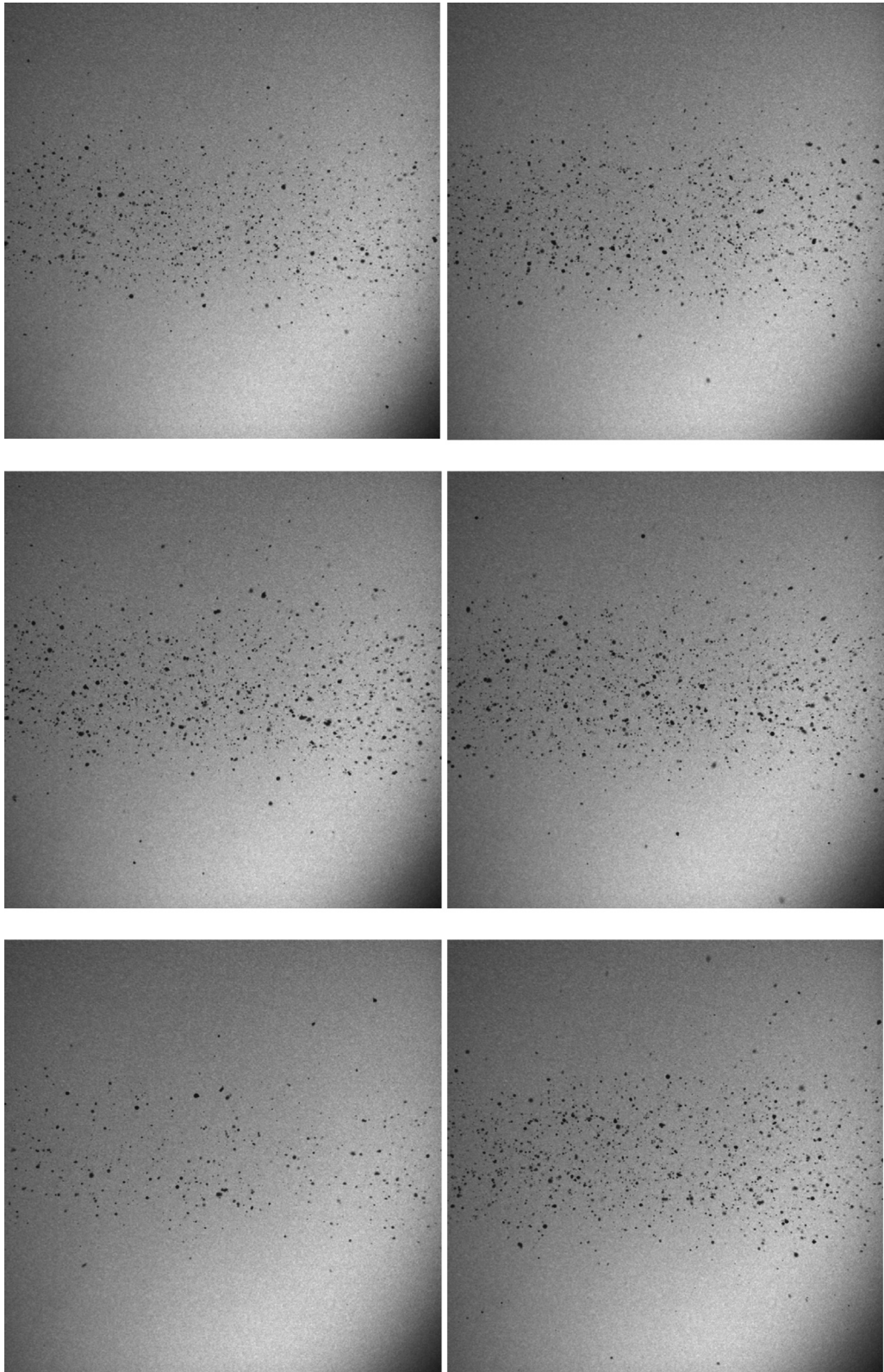


**Fig. 6.** Sequential stacking of 15 images that shows the onset of typical randomly and non-repetitive dispersion within zone 3.

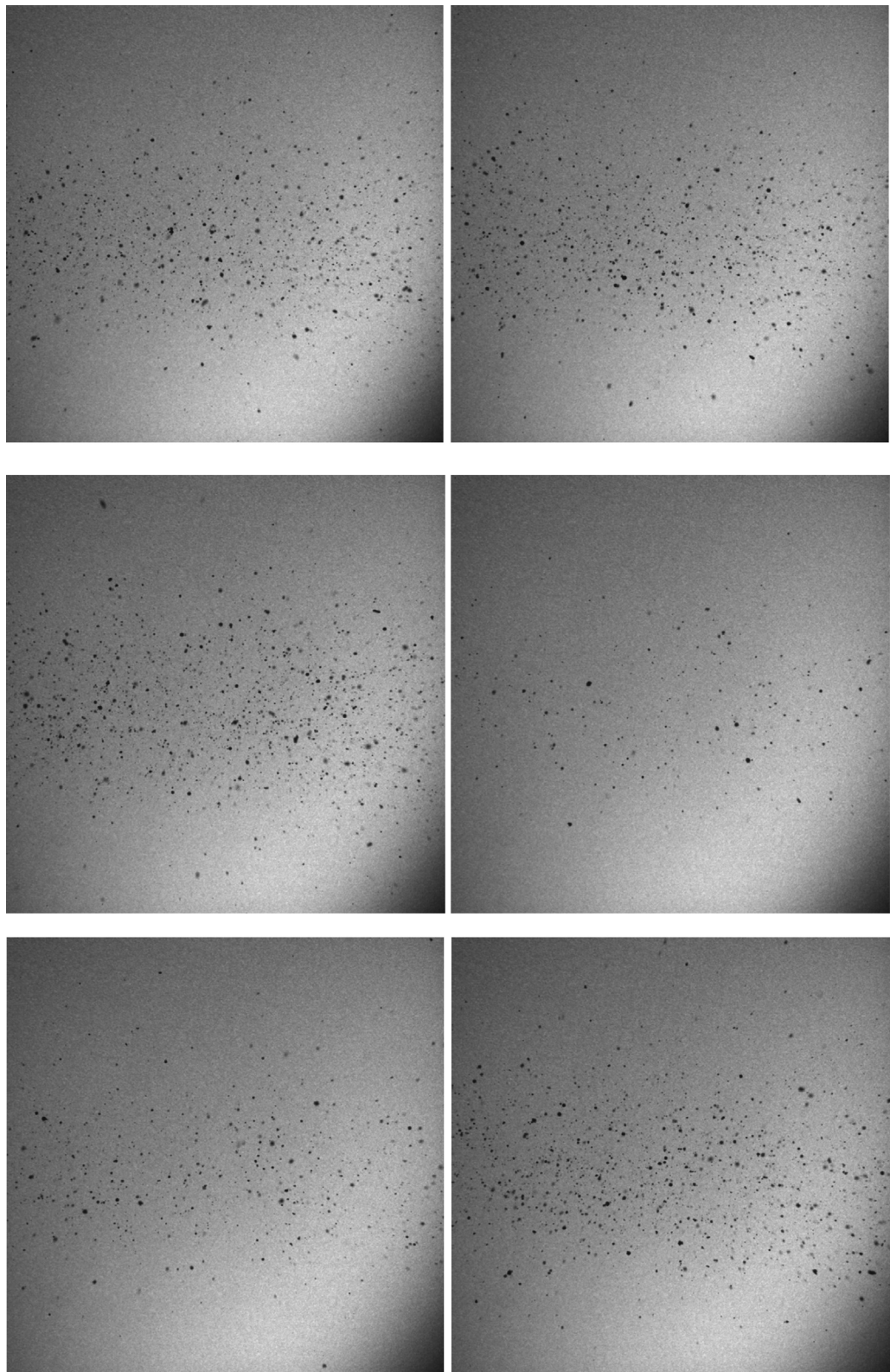


**Fig. 7.** Sequential stacking of 15 images that shows typical development of random and non-repetitive significant dispersion at the zone 5.

weak size, the particles are lightweight enough to be sensitive to a fluid flow disturbance. Micron powders can also be sensitive to gravity effect, but mostly when they are exposed to a low velocity range for which spatial selective deposition may occur [29,30]. The flow regime in cold spraying is however supersonic

over a large distance ahead the nozzle so that the inertial effect due the gas flow is predominant and governs the particles kinematics. Thus, the dispersed pattern of the powders outside the nozzle is rather attributed to a turbulent behaviour of the gas flow.

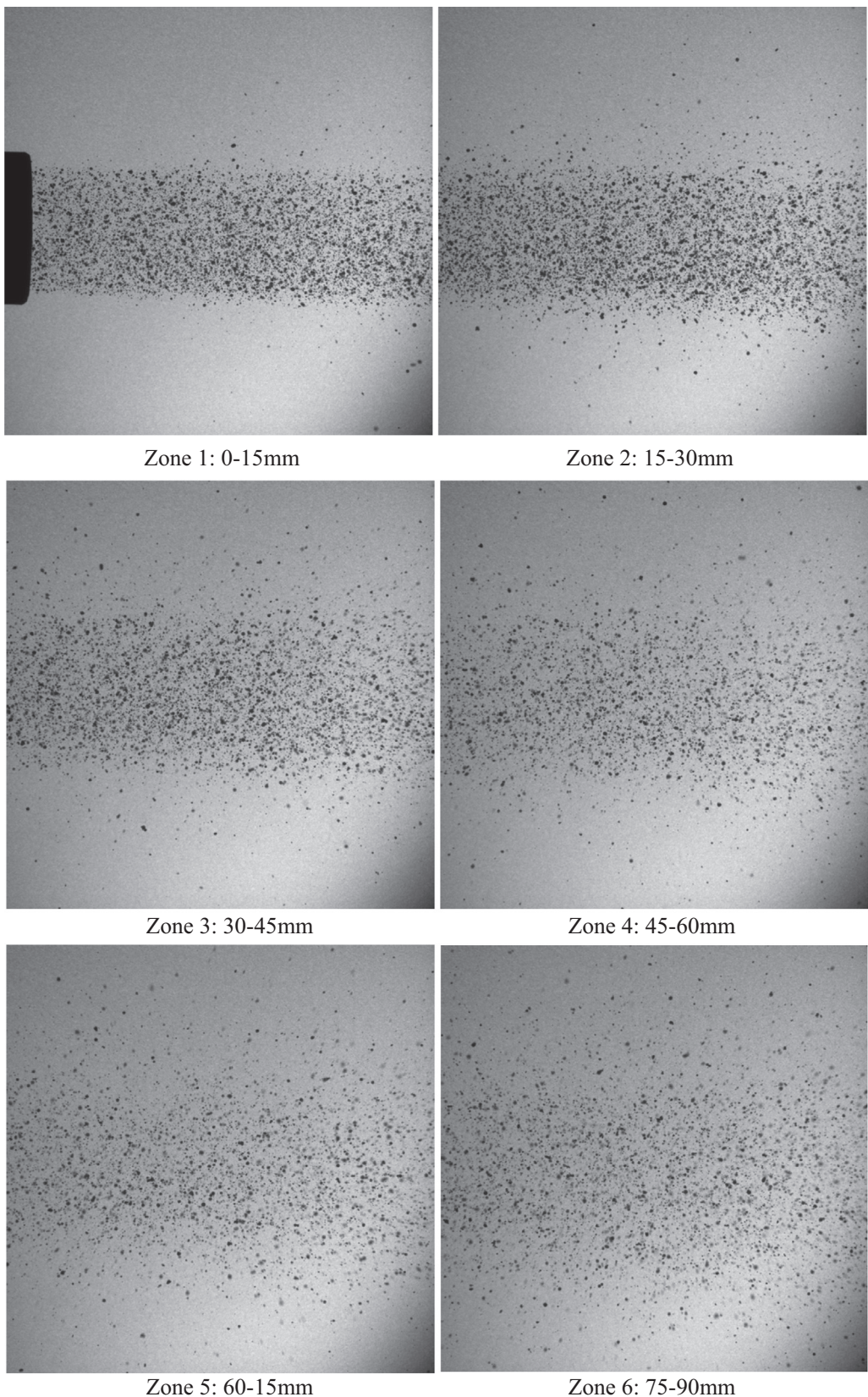


**Fig. 8.** Sequential stacks of 100 images over a duration of 5 s providing a global visualization of the particle's location and flow pattern from zone 1 to zone 6.

### 3.2. Quantitative characterization of the particles jet regime

A stacking of 100 images over a duration of 5 s provides a global visualization of the particle's location and flow pattern that leads to a good identification of the global kinematic behaviour of the particles within each zone. The phenomenon of continuous particles dispersion causes a transition from the regular flow pattern into a disperse flow as clearly revealed in Fig. 8. The particles scattering increases at zone 2 and becomes prominent from zone 3. More and more particles radially deviate from zone 2 and the central jet is less and less dense with the progression of the flow. The particles jet is completely sparse at zone 6. The phenomenological flow of the particles along the flow direction outside the nozzle is then characterized by a consecutive variance of the jet, uniform at

first, and then weakly disperse to become completely sparse after. Quantitative characterization of this jet variance is suggested using the greyscale of each pixel of the stacked images. Since the shadows generated by the particles are dark, they are encoded by high grey level in contrast with low grey level value of the grey background. Thus, the grey transition across the particles pixels produces peak values whose position enables for measuring the diameter of the particles jet along the flow direction. Fig. 9a presents typical variations of grey levels across the particles jet at the onset of each zone that quantifies the radial confinement of the particles in zone 1, and then the range of radial dispersion while the particles progress from zone 2 to zone 6. The axial variation of the radial distribution of particles gives the particles jet diameter across the uniform flow pattern within zone 1 towards

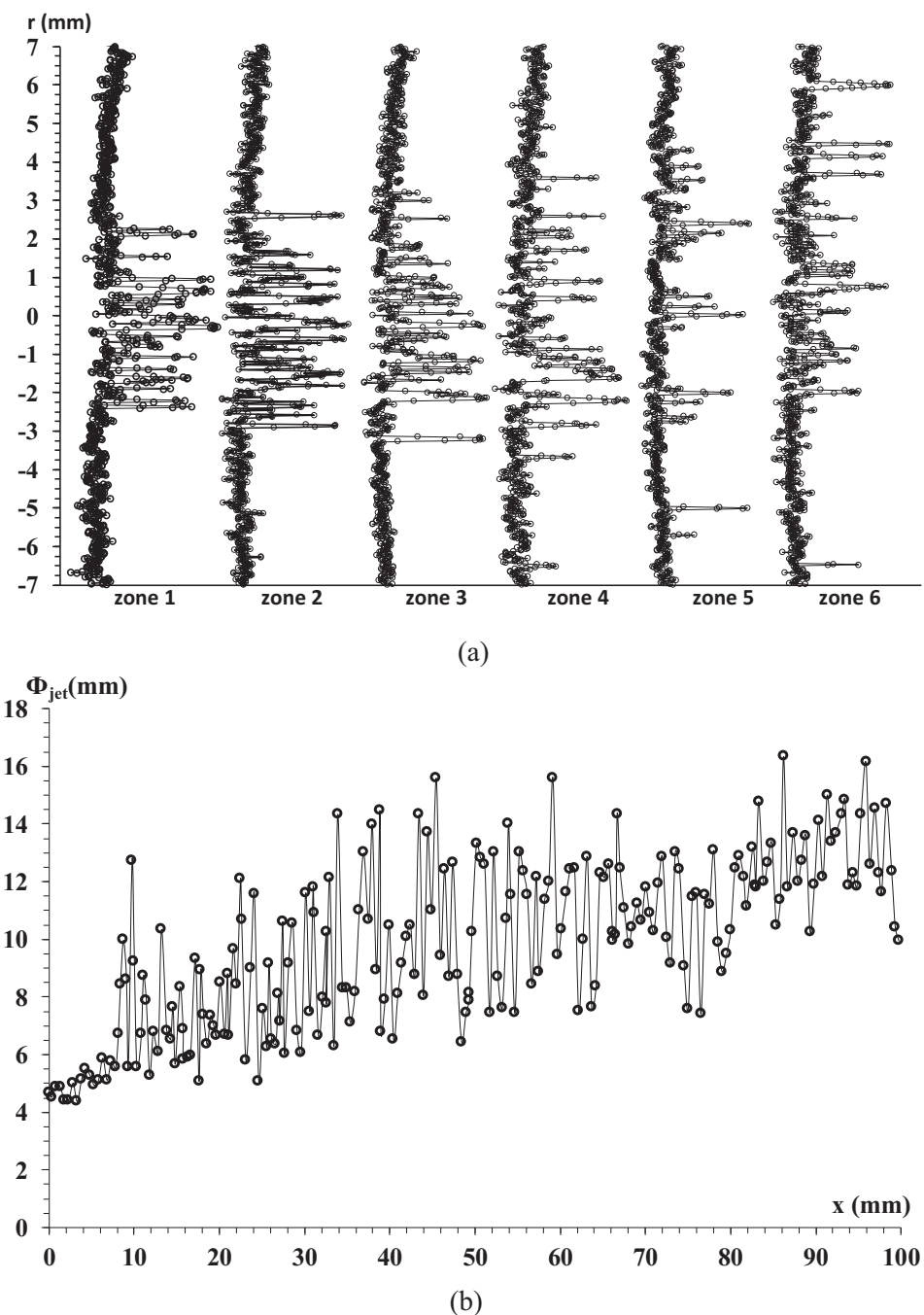


**Fig. 9.** Typical variations of grey levels across the particles jet, at the onset of each zone (a), that enables the assessment of the particles jet along the flow direction (b).

the zones of dispersed flow (Fig. 9b). Thus, a critical distance ( $D_{cr}$ ) in terms of a uniform jet can be identified which is less than 10 mm for the case of the large copper. The irregular variation of the jet diameter due to the dispersion beyond  $D_{cr}$  makes tricky the use of this diameter for well characterizing the dispersed jet. The radial dispersion of the particles along the axial direction is random so that it is rather suitable for providing a tendency of dispersion widening. Instead, we can consider the presence of particles inside the central zone of the jet. The diameter of the nozzle exit is used as the boundary of this zone.

Fig. 10 plots the proportion of particles that remain in the central zone along the axial direction of the flow. Although dispersion starts at zone 1, nearly 100% of the particles stay inside the central zone while a very few proportions only are deviated outward. The central zone still contains a large proportion of particles at zone 2, higher than 90%, albeit the jet diameter formed by the dispersed particles quickly becomes significant. The criterion of uniform jet does not longer prevail but the proportion of high particles can be considered as another criterion to suggest this zone 2 as suitable standoff distance free of strong dispersion which becomes significant from zone 4 to zone 6 where the proportion of outward dispersed particles reaches up to about 30%. Therefore, the particles jet is fully dispersing for large deposition distance whereas short standoff distance less than 30 mm in this case of large copper can produce less sparse jet with a weak particle deviation. Working at high standoff distance promotes thereby a particle dispersion phenomenon which can impair the deposition. The particles deviation generates oblique collision onto the substrate that has a negative effect according to the literature. Depositions with various spraying angles show that increasing the oblique collision decreases the DE, the coating thickness and the adhesion capability. High spraying angles even prevent the adhesion of the particles onto the substrate due to a rebounding involved by the tangential inertia during the oblique impact [21–26]. This effect implies to well depict the dispersion occurrence for LPCS in case of fine particles that is suggested to gain kinematic efficiency [14].

Dispersions of particles more lightweight than the large copper case is also plotted on Fig. 10. The results are similar in terms of the progression of particles proportion inside the central zone along

the flow direction. There is a general decrease in this proportion from zone 1 to zone 6. Also, the lighter the powders, the less the proportion value, that is, the more disperse the particles stream due to more sensitivity to the gas flow fluctuation. The comparison between the cases Cu\_2, Cu\_1, Al, and Mg evidences this dispersion behaviour. The case of Mg powders shows a typical strong sensitivity that involves a difficult apprehension of the particles flow. With the zone 1, their proportion is obviously less compared to both cases Cu\_2 and Cu\_1 but high compared with the case Al. Since they are lighter than these powders, they are more sensitive to the strong gas stream at the nozzle exit where they are confined while leaving the nozzle. Then, from zone 2, they exhibit the weakest proportion value in the centreline zone because of their higher sensitivity to the gas flow fluctuation. Extreme sensitivity in case of very fine powders (PEEK and WC-Co) shows however higher proportion values of particles in the central zone. Despite being very small, these fine particles are not dispersing like the lightweight Mg powders but present less dispersion comparable to that of heavier particles (Cu\_1). The behaviour of very light powders becomes thereby trickier to identify because of this non-linear particles' response. The next section brings qualitative depiction of the

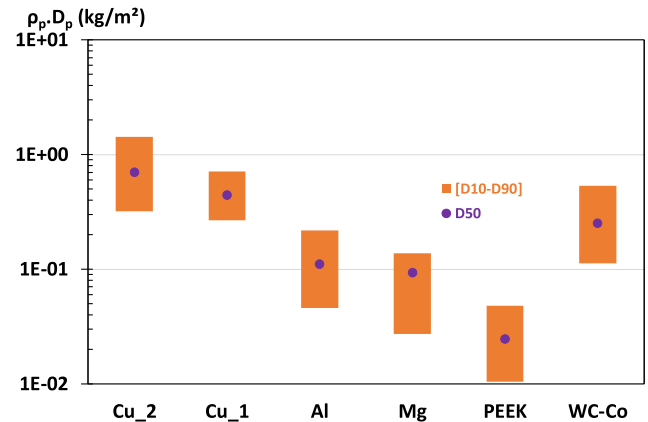


Fig. 11. Experimental range of  $\rho_p D_p$  that depicts the variance of lightness.

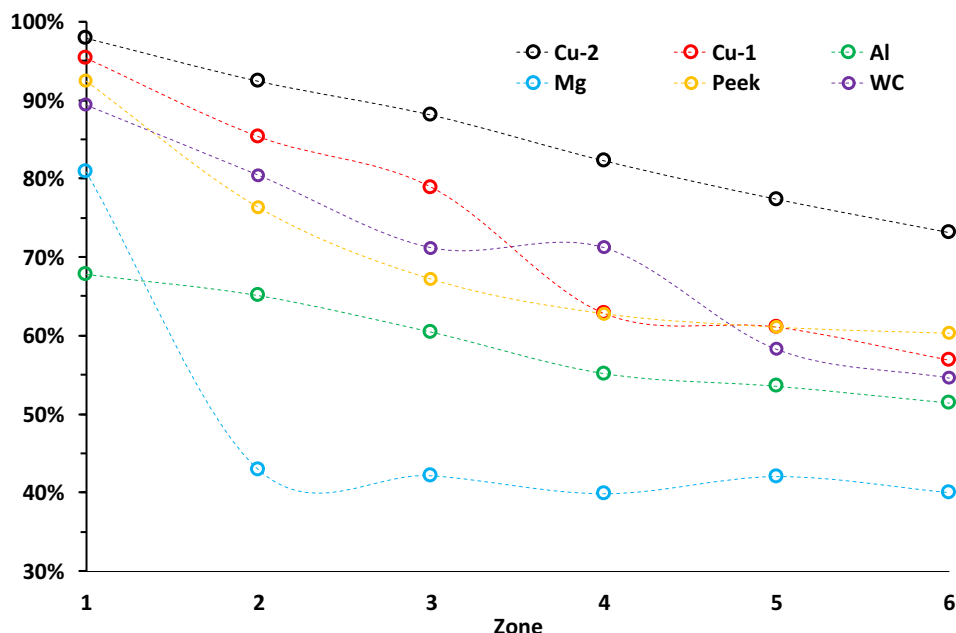
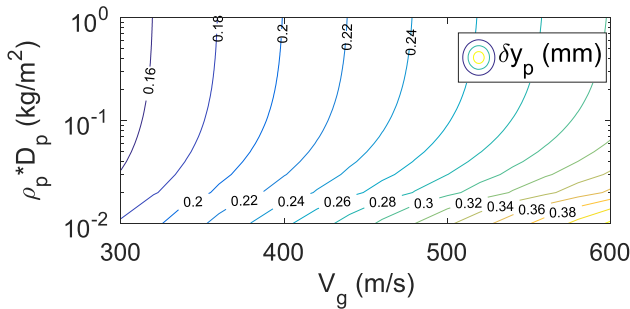


Fig. 10. Proportion of particles that remain in the central zone along the flow direction.



**Fig. 12.** Computed variance of  $\delta y_p$  due to the effect of both particle lightness and gas velocity.

particles' response using a simplified analytical law. The particles jet variance found with the experimental observation of the various powders (Cu\_2, Cu\_1, Al, Mg, PEEK and WC-Co) will be completed.

### 3.3. Effect of particles features on the jet development: Qualitative depiction and experimental variance

Basically, the size or the density of the particles governs their in-flight behaviour. The motion of a particle described by the kinematic Newton's law gathers these both parameters into a single term  $\rho_p D_p$  that is better to represent a global effect of particle lightness due to changes in  $\rho_p$  and  $D_p$ . Using this term is suitable for

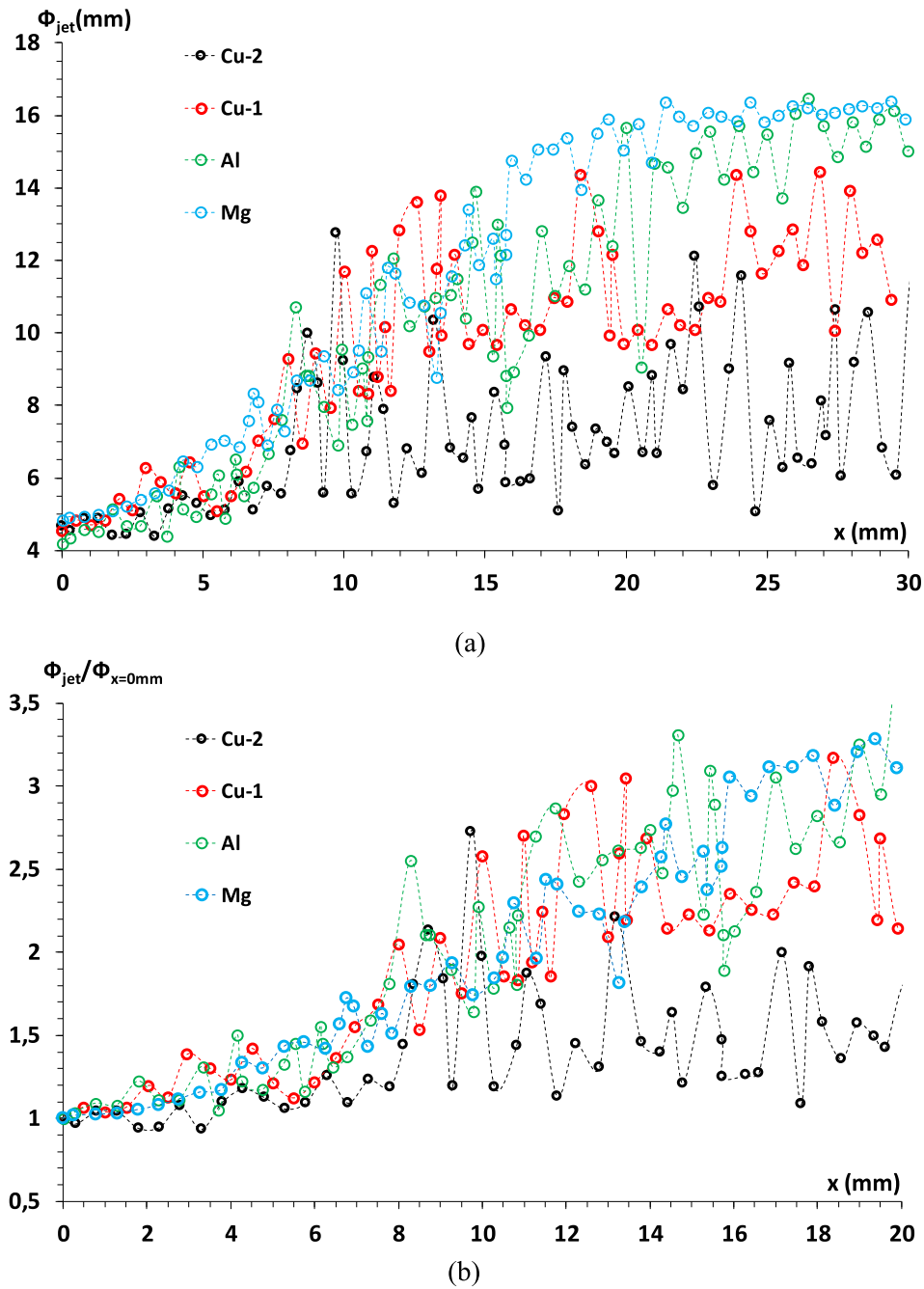


**Fig. 13.** Variation of particles jet diameter along with the flow direction (a), and ratio with respect to the value of the jet diameter immediately at the nozzle exit (b).

comparing the effect of both particle size and material density on the particle kinematics. Fig. 11 presents the experimental range of  $\rho_p D_p$  that depicts the variance of lightness below the case (Cu\_2). The lightweight nature of the powders becomes more and more significant across the variance of Cu\_1, Al, Mg, and PEEK. Note that despite the WC-Co powders are finely sized as the PEEK powders, they are however less lightweight with a  $\rho_p D_p$  value closed to the case Al, using the density of tungsten as computational data.

The analytical solution of the Newton's law of motion [17] enables a depiction of the particles kinematics due to both variances of  $\rho_p D_p$  and change in gas velocity. The incremental variation of the particle position, denoted  $\delta y_p$ , is described by the correlation (Eq. (1)).  $\delta y_p$  is computed using a typical range of nitrogen supersonic velocity in LPSCS (300–600 m/s).  $\delta t$  is the residence time (during reaching  $\delta y_p$ ) we prescribe a typical value of about 5  $\mu$ s that corresponds to the Mach number range of 1–2 in LPSCS [17]. The drag coefficient is fixed with a constant value of 0.4 used for spherical geometry.  $V_{p0}$  is the particle velocity value when  $\delta y_p = 0$ . This initial value is defined by a simple approximation depending on the gas velocity as follows  $V_{p0} = \alpha V_g$  using a weak value of the coefficient  $\alpha$  ( $\alpha = 0.1$ ).

$$\delta y_p = V_g \delta t - \frac{4}{3} \frac{\rho_p}{\rho_g} \frac{D_p}{C_D} \log \left[ 1 + \frac{3}{4} \frac{\rho_g}{\rho_p} \frac{C_D}{D_p} \delta t (V_g - V_{p0}) \right] \quad (1)$$

where  $\rho_g$  is the gas density and  $V_g$  is the gas velocity.

Fig. 12 displays the computed variance of  $\delta y_p$ . Basically, for any  $V_g$ ,  $\delta y_p$  increases while decreasing  $\rho_p D_p$ , that explains the particles are more sensitive to deviation, the more they are lightweight. The experimental dispersion fits in with this generic particle response. In the dispersion zone, the diameter of the particles jet increases from the heavy case Cu\_2 up to the lightweight case Mg, over the case Cu\_1 and then the case Al. However, before the particles get sparse, the size of the stable jet ahead of the nozzle is similar. At the nozzle exit, the cases Cu\_2, Cu\_1, Al and Mg exhibit a jet diameter of about 4 mm which is straight without significant devi-

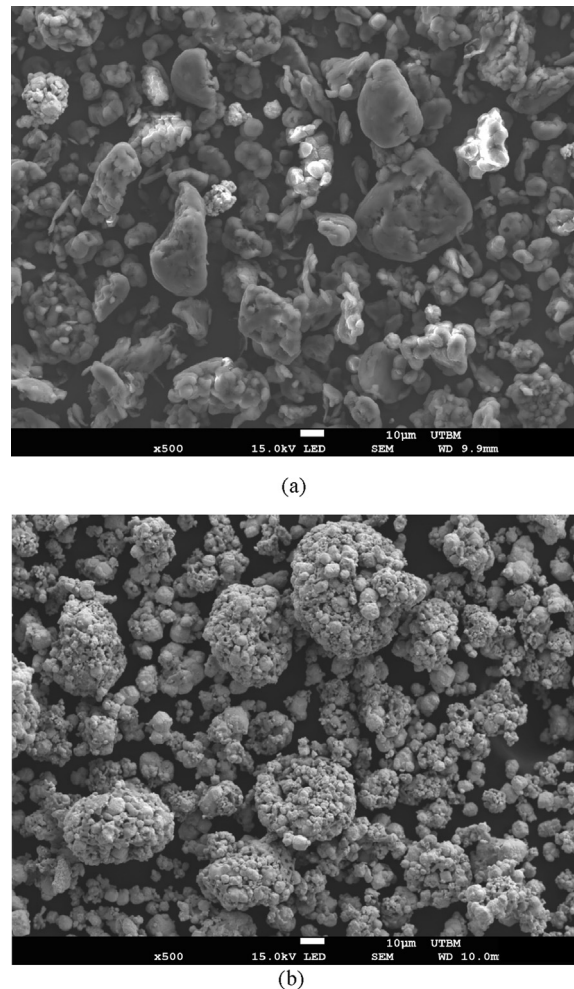


**Fig. 15.** Irregular shape of the PEEK powders (a), and porous feature of the WC-Co powders (b).

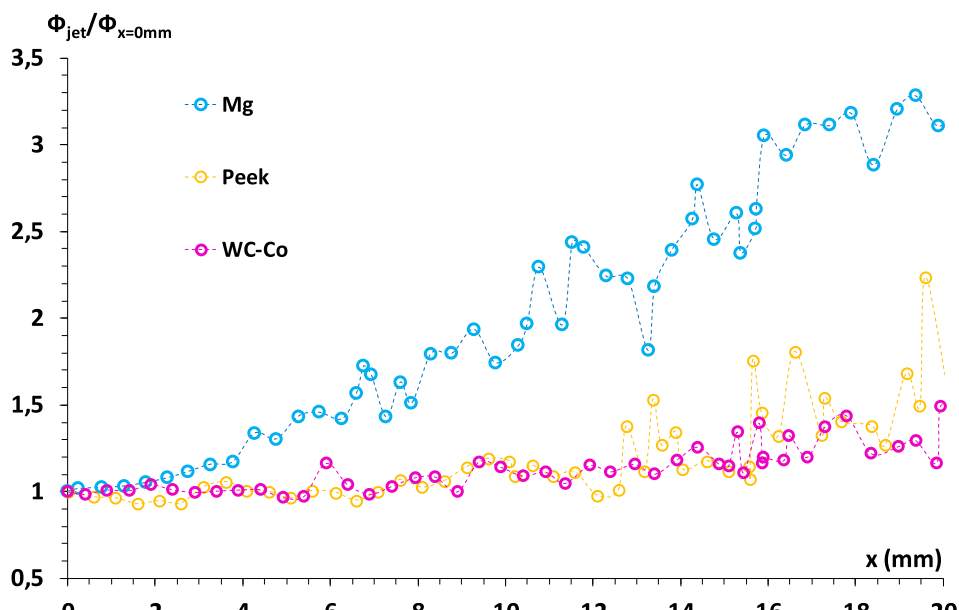


**Fig. 14.** Typical effect of lightweight particles on the particles flow: better stability of the PEEK powders and WC-Co powders compared to the Mg powders.

ation over a short distance (Fig. 13). The length of this distance can be characterized using the variation of jet diameter along the flow direction with respect to the value of the jet diameter immediately at the nozzle exit ( $x = 0$  mm). We denote this ratio  $\phi_{jet}/\phi_{x=0mm}$  which gives a good discussion on how straight the jet is while leaving the nozzle. Assuming a weak deviation closed to 1 (0.9–1.1) as a criterion of uniform jet, the results computed on Fig. 13 evidence a zone of straight jet less than 4 mm for the cases Cu\_2, Cu\_1, Al and Mg. However, these tendencies of particle response while decreasing  $\rho_p D_p$  across the variation (Cu\_2, Cu\_1, Al, Mg) cannot be extrapolated for depicting the situation of lighter particles. The typical dispersion that is expected to occur for lightweight particles as revealed by the case Mg does no longer prevail. The behaviour of the PEEK powders is completely different despite the  $\rho_p D_p$  value of PEEK is below the case of Mg powders.

For the PEEK powders, the distance of stable particles jet is at least four times higher than the case of Mg powders and the dispersion is also weaker within the unstable jet zone (Fig. 14). The PEEK powders are more stable and last longer in the central jet due to a sensitivity to the axial velocity of the gas. The more inertial effect occurs in this direction and the lightness of the PEEK powders promotes this axial motion instead of a radial deviation that appears in the case of Mg powders that have more radial inertia. In addition, the PEEK powders are not spherical but have an irregular morphology (Fig. 15a). This feature promotes a fast separation of the boundary layer over the powder surface during the in-flight motion, and thus a negative pressure gradient that enables the particle to reach more inertial effect [27,31,32]. The irregularly shaped powders are found to have the highest inertial effect and then the highest in-flight velocities [19,33]. Due to this increased inertial effect combined with a weak  $\rho_p D_p$ , the axial component of  $V_g$  ( $V_{gx}$ ) rather involves a confinement of the fine angular particles such as PEEK in the central zone of the jet. Since  $V_{gx}$  progressively decreases along the flow direction within the atmospheric media outside the nozzle, there is an incremental sensitivity to the radial component of  $V_g$  so that the particles become to be dispersed beyond larger distance of about 12 mm (Fig. 14). Compared with the PEEK case, the WC-Co case is more stable. Both are similar in size, but the feature of the agglomerated nearly spherical WC-Co

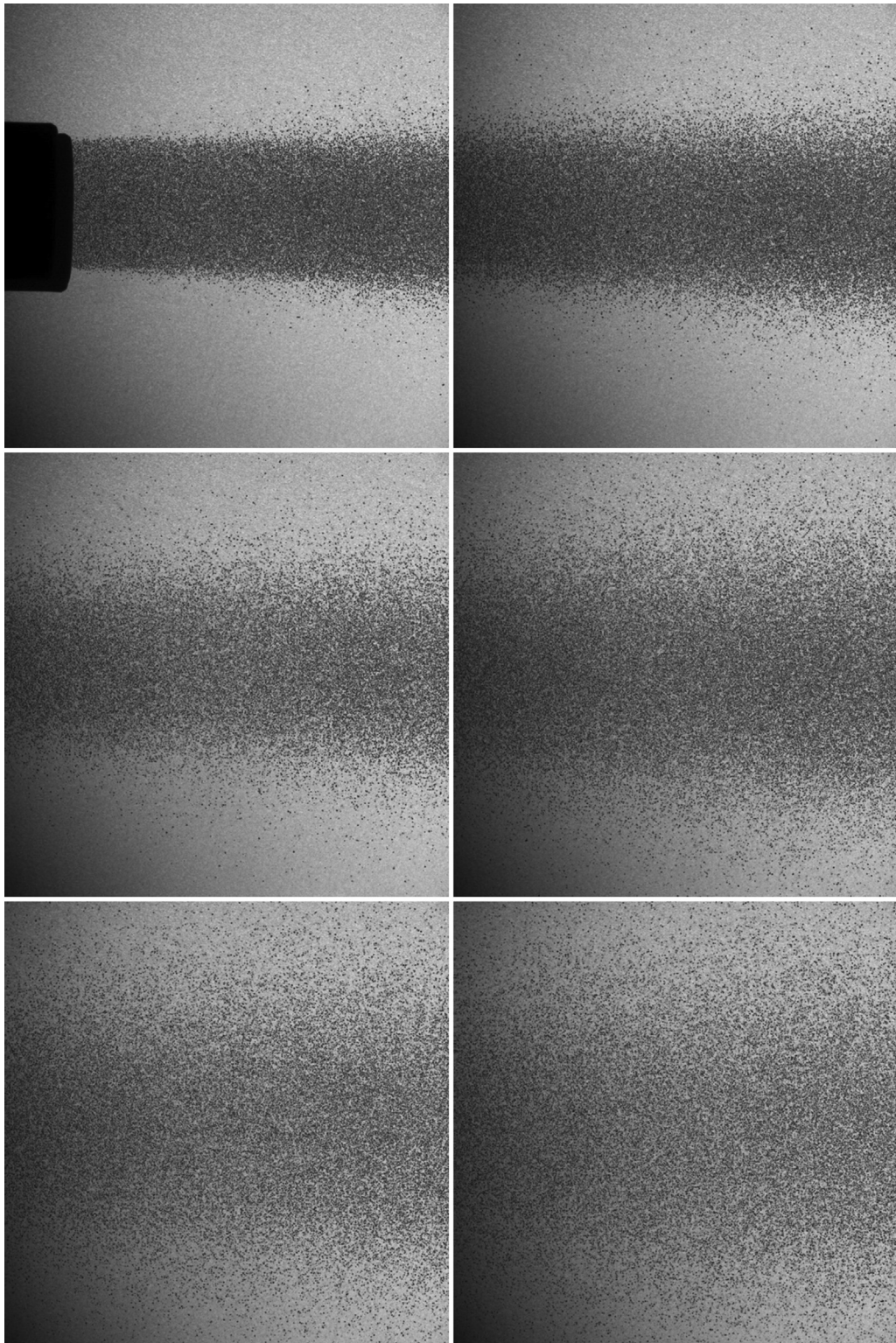
powders makes tricky the comparison of these PEEK and WC-Co particles in term of reliable  $\rho_p D_p$ . The real density of the WC-Co powders is difficult to assess due to its porous nature (Fig. 15b). However, the better stability of the WC-Co powders can be attributed to two consequences of this pores feature: a lightness effect due to real density smaller than the PEEK, and/or a better inertial effect due to the irregular morphology the pores create over the surface of the WC-Co powders. Together, these kinematic results show a difficulty to obtain a particle flow free of dispersion for standoff distances that are widely enacted in cold spraying, in the range of 10–50 mm [27]. Optimizing the DE requires also to identify the suitable standoff distance which can minimize the particles deviation to prevent oblique collisions due to their negative consequences on the DE and the coating features [21–26].

#### 4. Conclusions

The kinematic behaviour of particles during low pressure cold spraying are investigated using experimental shadowgraph analysis. There is a generic behaviour of the powders flow, that is, a straight jet over a certain distance and then a dispersed flow. Both onset distance and widening of the dispersion depend on the powder nature that can be depicted by effects of  $\rho_p D_p$  including various representative cases: high  $\rho_p D_p$  using large copper, intermediate cases with finer copper, aluminium powders and magnesium powders, and low  $\rho_p D_p$  using very fine powders of PEEK and WC-Co. The less  $\rho_p D_p$ , the more sensitive to deviation are the particles and the strongest is the dispersion. The distance of straight jet is about 5 mm, except for the low  $\rho_p D_p$  case. This tendency is no longer valid for the PEEK powders because they stay longer in the central jet and develop large distance of stable zone, of about 20 mm. This better stability is attributed to higher axial inertia caused by the axial component of the gas immediately outside the nozzle exit. The PEEK powders get unstable later along the flow direction due to an increased sensitivity to the radial component of the gas velocity while the axial velocity of the gas progressively collapses within the outer atmospheric media. The fine WC-Co powders behave like the PEEK powders since they are also lightweight due to the porous feature of each particle.

**Appendices A. High-speed shadowgraph visualization of the other powder flows**

(See Figs. A1–A5).

**Fig. A1.** Phenomenological flow of the case Cu\_1 from zone 1 to zone 6.

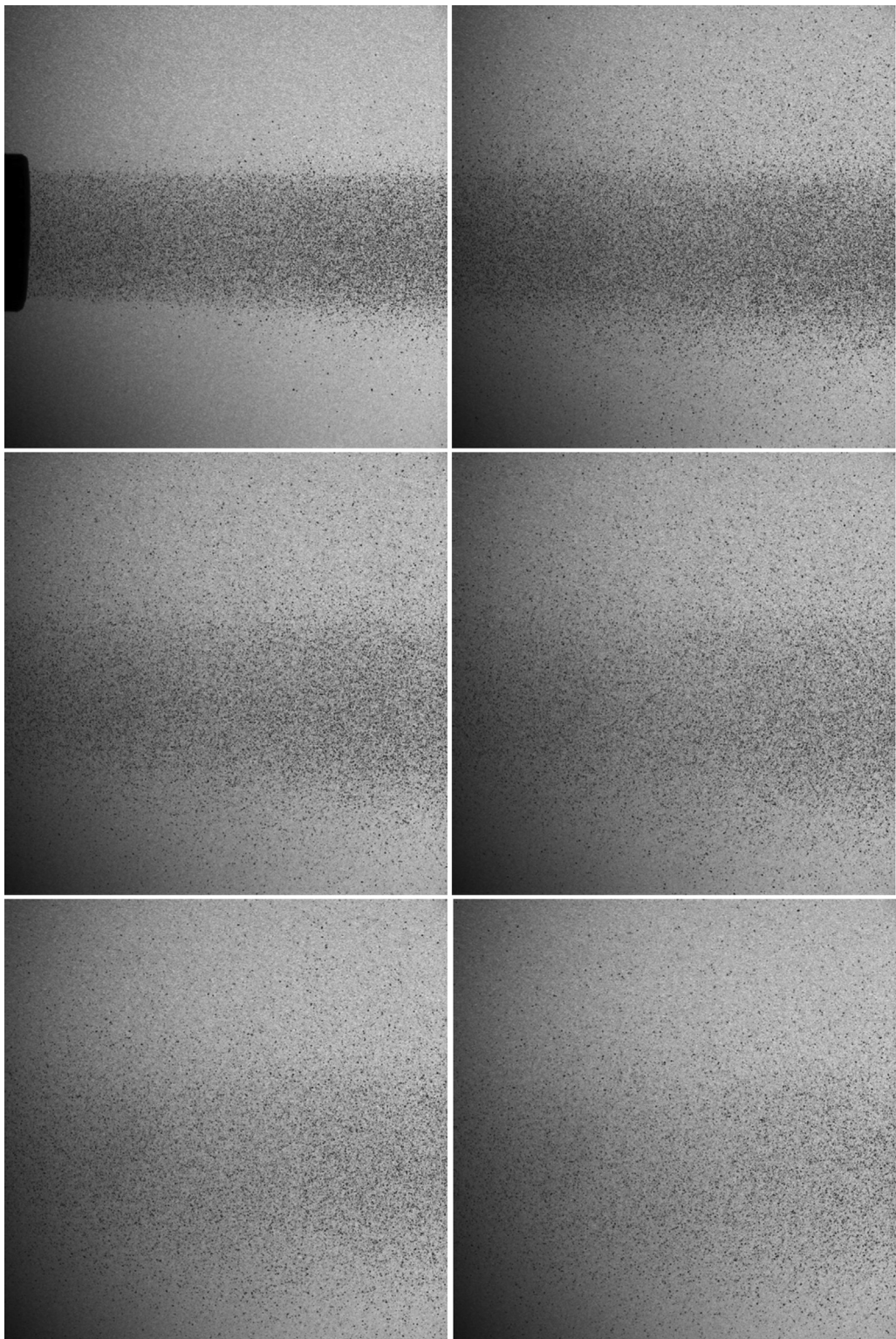


**Fig. A2.** Phenomenological flow of the case Al from zone 1 to zone 6.

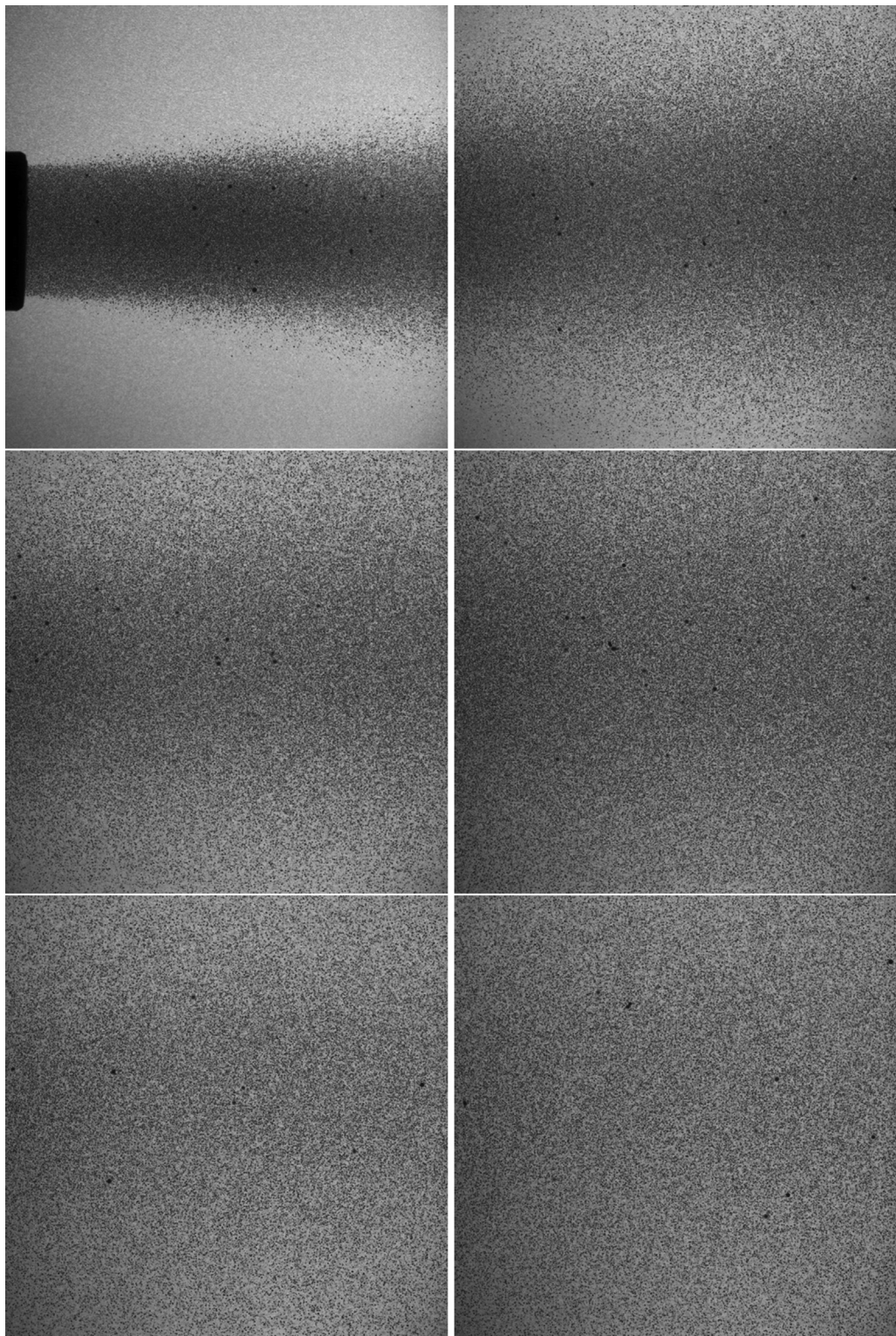


**Fig. A3.** Phenomenological flow of the case Mg from zone 1 to zone 6.

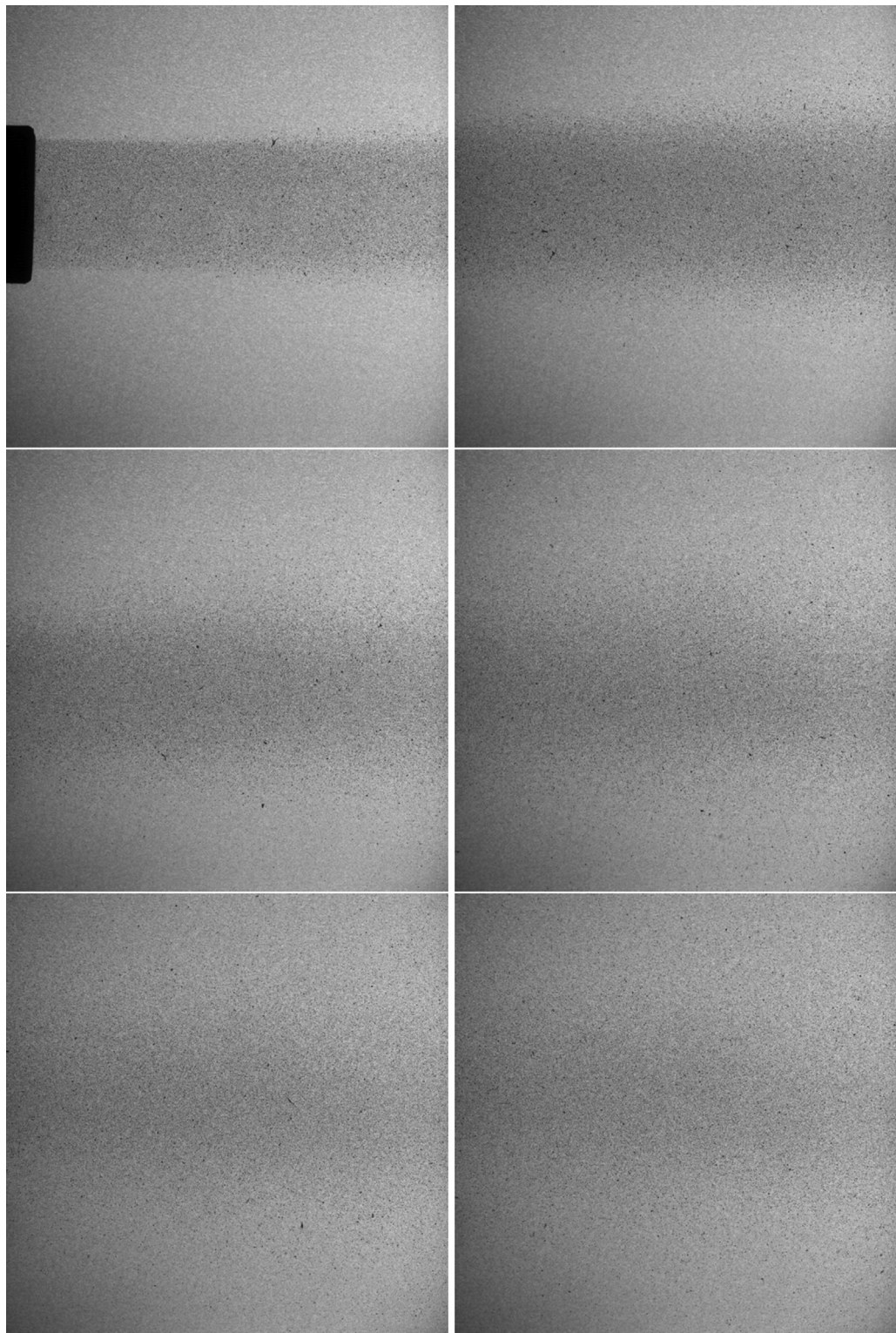


**Fig. A4.** Phenomenological flow of the case PEEK from zone 1 to zone 6.

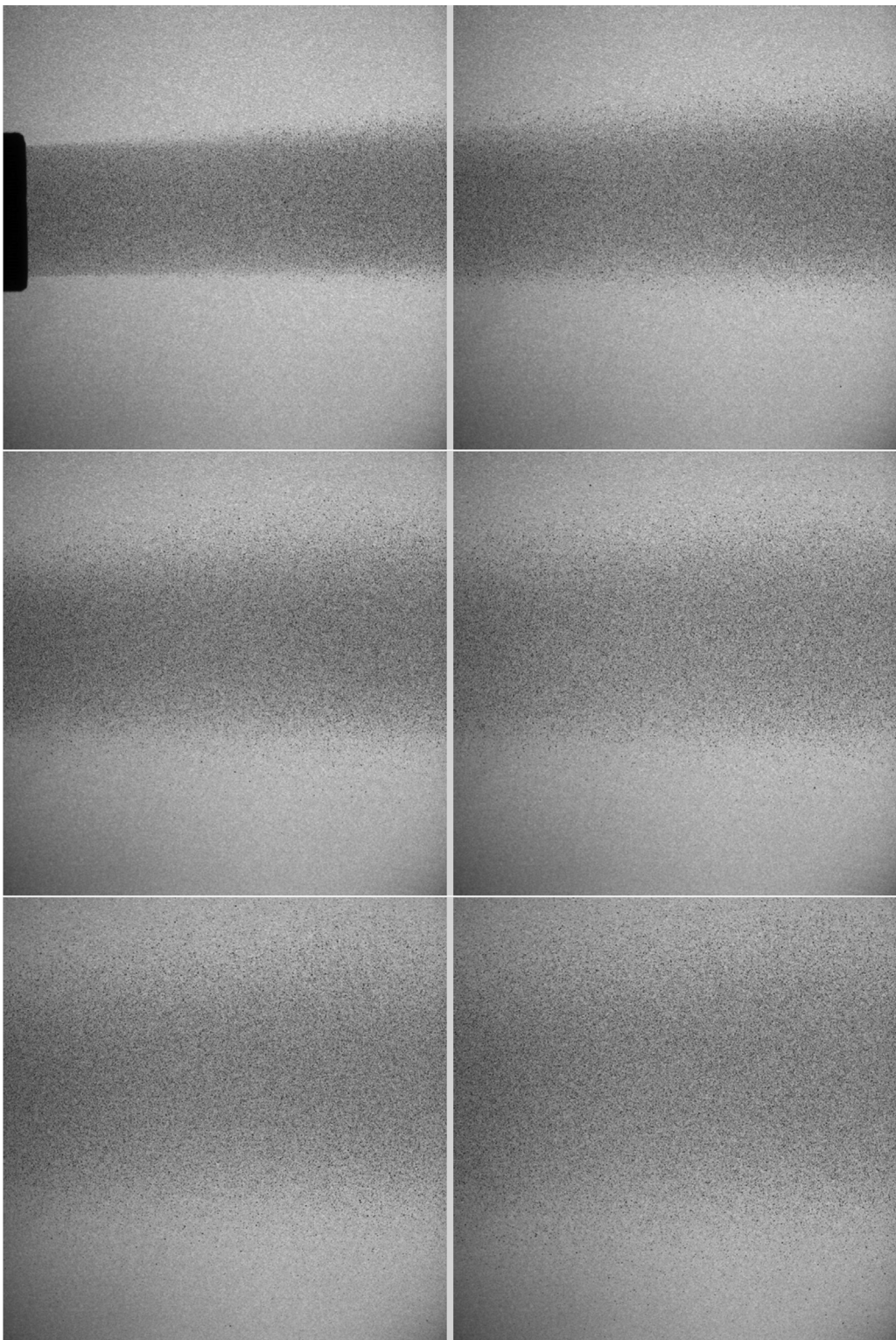


**Fig. A5.** Phenomenological flow of the case WC-Co from zone 1 to zone 6.

## References

- [1] A. Moridi, S.M. Hassani-Gangaraj, M. Guagliano, M. Dao, Cold spray coating: review of material systems and future perspectives, *Surf. Eng.* 30 (2014) 369–395.
- [2] R.N. Raoelison, Coeval Cold spray additive manufacturing variances and innovative contributions, in: *Cold-Spray Coat.*, Springer, Cham, 2018, pp. 57–94, [https://doi.org/10.1007/978-3-319-67183-3\\_3](https://doi.org/10.1007/978-3-319-67183-3_3).
- [3] H. Assadi, H. Kreye, F. Gärtner, T. Klassen, Cold spraying – A materials perspective, *Acta Mater.* (n.d.). <https://doi.org/10.1016/j.actamat.2016.06.034>.
- [4] R.N. Raoelison, Ch. Verdy, H. Liao, Cold gas dynamic spray additive manufacturing today: Deposit possibilities, technological solutions and viable applications, *Mater. Des.* 133 (2017) 266–287, <https://doi.org/10.1016/j.matdes.2017.07.067>.
- [5] I. Burlacov, J. Jirkovský, L. Kavan, R. Ballhorn, R.B. Heumann, Cold gas dynamic spraying (CGDS) of TiO<sub>2</sub> (anatase) powders onto poly(sulfone) substrates: Microstructural characterisation and photocatalytic efficiency, *J. Photochem.*

- Photobiol. Chem. 187 (2007) 285–292, <https://doi.org/10.1016/j.jphotochem.2006.10.023>.
- [6] D. Seo, M. Sayar, K. Ogawa, SiO<sub>2</sub> and MoSi<sub>2</sub> formation on Inconel 625 surface via SiC coating deposited by cold spray, Surf. Coat. Technol. 206 (2012) 2851–2858, <https://doi.org/10.1016/j.surfcoat.2011.12.010>.
- [7] R. Lupoi, W. O'Neill, Deposition of metallic coatings on polymer surfaces using cold spray, Surf. Coat. Technol. 205 (2010) 2167–2173, <https://doi.org/10.1016/j.surfcoat.2010.08.128>.
- [8] F. Robitaille, M. Yandouzi, S. Hind, B. Jodoin, Metallic coating of aerospace carbon/epoxy composites by the pulsed gas dynamic spraying process, Surf. Coat. Technol. 203 (2009) 2954–2960, <https://doi.org/10.1016/j.surfcoat.2009.03.011>.
- [9] X.L. Zhou, A.F. Chen, J.C. Liu, X.K. Wu, J.S. Zhang, Preparation of metallic coatings on polymer matrix composites by cold spray, Surf. Coat. Technol. 206 (2011) 132–136, <https://doi.org/10.1016/j.surfcoat.2011.07.005>.
- [10] A. Ganesan, J. Affi, M. Yamada, M. Fukumoto, Bonding behavior studies of cold sprayed copper coating on the PVC polymer substrate, Surf. Coat. Technol. 207 (2012) 262–269, <https://doi.org/10.1016/j.surfcoat.2012.06.086>.
- [11] R.N. Raeelson, L.L. Koithara, S. Costil, X. Xie, Capability of cold spraying to obtain high deposition efficiency for the metallization of PEEK, in: Asm, 2019, <https://asm.confex.com/asm/itsc19/webprogram/Paper47021.html> (accessed November 27, 2019).
- [12] P.C. King, A.J. Poole, S. Horne, R. de Nys, S. Gulizia, M.Z. Jahedi, Embedment of copper particles into polymers by cold spray, Surf. Coat. Technol. 216 (2013) 60–67, <https://doi.org/10.1016/j.surfcoat.2012.11.023>.
- [13] A.S. Alhulaifi, G.A. Buck, W.J. Arbegast, Numerical and experimental investigation of cold spray gas dynamic effects for polymer coating, J. Therm. Spray Technol. 21 (2012) 852–862, <https://doi.org/10.1007/s11666-012-9743-4>.
- [14] R.N. Raeelson, E. Aubignat, M.-P. Planche, S. Costil, C. Langlade, H. Liao, Low pressure cold spraying under 6 bar pressure deposition: Exploration of high deposition efficiency solutions using a mathematical modelling, Surf. Coat. Technol. 302 (2016) 47–55, <https://doi.org/10.1016/j.surfcoat.2016.05.068>.
- [15] K. Ogawa, K. Ito, K. Ichimura, Y. Ichikawa, S. Ohno, N. Onda, Characterization of low-pressure cold-sprayed aluminum coatings, J. Therm. Spray Technol. 17 (2008) 728–735, <https://doi.org/10.1007/s11666-008-9254-5>.
- [16] V. Gillet, E. Aubignat, S. Costil, B. Courant, C. Langlade, P. Casari, W. Knapp, M.P. Planche, Development of low pressure cold sprayed copper coatings on carbon fiber reinforced polymer (CFRP), Surf. Coat. Technol. (2019), <https://doi.org/10.1016/j.surfcoat.2019.01.011>.
- [17] R.N. Raeelson, Analytical description of solid particles kinematics due to a fluid flow and application to the depiction of characteristic kinematics in cold spraying, Powder Technol. 319 (2017) 191–203, <https://doi.org/10.1016/j.powtec.2017.06.029>.
- [18] R.C. Dykhuizen, M.F. Smith, Gas dynamic principles of cold spray, J. Therm. Spray Technol. 7 (1998) 205–212, <https://doi.org/10.1361/105996398770350945>.
- [19] X.-J. Ning, J.-H. Jang, H.-J. Kim, The effects of powder properties on in-flight particle velocity and deposition process during low pressure cold spray process, Appl. Surf. Sci. 253 (2007) 7449–7455, <https://doi.org/10.1016/j.apsusc.2007.03.031>.
- [20] A.P. Alkhimov, V.F. Kosarev, A.N. Papyrin, A method of cold gas-dynamic deposition, Sov. Phys. Dokl. 35 (1990) 1047.
- [21] D.L. Gilmore, R.C. Dykhuizen, R.A. Neiser, T.J. Roemer, M.F. Smith, Particle velocity and deposition efficiency in the cold spray process, J. Therm. Spray Technol. 8 (1999) 576–582, <https://doi.org/10.1361/105996399770350278>.
- [22] K. Binder, J. Gottschalk, M. Kollenda, F. Gärtner, T. Klassen, Influence of impact angle and gas temperature on mechanical properties of titanium cold spray deposits, J. Therm. Spray Technol. 20 (2011) 234–242, <https://doi.org/10.1007/s11666-010-9557-1>.
- [23] C.-J. Li, W.-Y. Li, Y.-Y. Wang, Effect of spray angle on deposition characteristics in cold spraying, in: Proc. Int. Therm. Spray Conf., C. Moreau and B. Marple, Orlando, Florida, 2003, pp. 91–96.
- [24] S. Yin, X. Su, J. Su, Z. Guo, H. Liao, X. Wang, Effects of substrate hardness and spray angle on the deposition behavior of cold-sprayed Ti particles, J. Therm. Spray Technol. 23 (2014) 76–83, <https://doi.org/10.1007/s11666-013-0039-0>.
- [25] R. Singh, K.-H. Rauwald, E. Wessel, G. Mauer, S. Schruefer, A. Barth, S. Wilson, R. Vassen, Effects of substrate roughness and spray-angle on deposition behavior of cold-sprayed Inconel 718, Surf. Coat. Technol. (n.d.). <https://doi.org/10.1016/j.surfcoat.2017.03.072>.
- [26] C.-J. Li, W.-Y. Li, H. Liao, Examination of the critical velocity for deposition of particles in cold spraying, J. Therm. Spray Technol. 15 (2006) 212–222, <https://doi.org/10.1361/105996306X108093>.
- [27] R.N. Raeelson, Y. Xie, T. Sapanathan, M.P. Planche, R. Kromer, S. Costil, C. Langlade, Cold gas dynamic spray technology: A comprehensive review of processing conditions for various technological developments till to date, Addit. Manuf. 19 (2018) 134–159, <https://doi.org/10.1016/j.addma.2017.07.001>.
- [28] R. Raeelson, L.L. Koithara, S. Costil, C. Langlade, Turbulences of the supersonic gas flow during cold spraying and their negative effects: a DNS CFD analysis coupled with experimental observation and laser impulse high-speed shadowgraphs of the particles in-flight flow, Int. J. Heat Mass Transf. 147 (2020) 118894, <https://doi.org/10.1016/j.ijheatmasstransfer.2019.118894>.
- [29] M. Rahimi-Gorji, O. Pourmehran, M. Gorji-Bandpy, T.B. Gorji, CFD simulation of airflow behavior and particle transport and deposition in different breathing conditions through the realistic model of human airways, J. Mol. Liq. 209 (2015) 121–133, <https://doi.org/10.1016/j.molliq.2015.05.031>.
- [30] M. Rahimi Gorji, L. Van de Sande, C. Debbaut, P. Segers, W. Willaert, W. Ceelen, Computational fluid dynamics model of pressurized intraperitoneal aerosols chemotherapy : gravity matters!, in: Proc. 2019 Summer Biomech. Bioeng. Biotransport Conf., SB3C Foundation, 2019. <http://hdl.handle.net/1854/LU-8609052> (accessed November 28, 2019).
- [31] B. Jodoin, L. Ajdelsztajn, E. Sansoucy, A. Zúñiga, P. Richer, E.J. Lavernia, Effect of particle size, morphology, and hardness on cold gas dynamic sprayed aluminum alloy coatings, Surf. Coat. Technol. 201 (2006) 3422–3429, <https://doi.org/10.1016/j.surfcoat.2006.07.232>.
- [32] N. Cinca, J.M. Rebled, S. Estradé, F. Peiró, J. Fernández, J.M. Guilemany, Influence of the particle morphology on the Cold Gas Spray deposition behaviour of titanium on aluminum light alloys, J. Alloys Compd. 554 (2013) 89–96, <https://doi.org/10.1016/j.jallcom.2012.11.069>.
- [33] W. Wong, P. Vo, E. Irissou, A.N. Ryabinin, J.-G. Legoux, S. Yue, Effect of particle morphology and size distribution on cold-sprayed pure titanium coatings, J. Therm. Spray Technol. 22 (2013) 1140–1153, <https://doi.org/10.1007/s11666-013-9951-6>.